# Near-infrared laser pumped intersubband THz laser gain in InGaAs-AlAsSb-InP quantum wells

Ansheng Liu* and C. Z. Ning

*NASA Ames Research Center, M/S N229-1, Moffett Field, CA 94035*

(November 17, 1999)

## Abstract

We investigate the possibility of using InGaAs-AlAsSb-InP coupled quantum wells to generate THz radiation by means of intersubband optical pumping. We show that large conduction band offsets of these quantum wells make it possible to use conventional near-infrared diode lasers around 1.55 $\mu$m as pump sources. Taking into account the pump-probe coherent interaction and the optical nonlinearity for the pump field, we calculate the THz gain of the quantum well structure. We show that resonant Raman scattering enhances the THz gain at low and moderate optical pumping levels. When the pump intensity is strong, the THz gain is reduced by pump-induced population redistribution and pump-probe coherent interactions.

The early proposal[1] and recent demonstration[2] of intersubband semiconductor quantum well (QW) lasers have aroused considerable interest because of their potential applications in the mid-infrared frequency range and because only electrons participate in the lasing process, which is different from the conventional semiconductor lasers based on interband transitions. Up to now, the electrically injected quantum cascade lasers have been very successful in the mid-infrared range.[3,4] The optically pumped intersubband lasers have also been demonstrated in the wavelength around 15 $\mu$m.[5,6] A natural question is whether the concept of the intersubband laser can be generalized to much longer wavelength preferably to 30-300 $\mu$m or THz range.[7–9] This question is especially interesting due to the current lack of solid-state THz sources and the enormous potential applications of such sources. Compared to the electrically injected lasers, the optically pumped lasers have advantages of easier realization of population inversion and less sophisticated device design. In addition, in the optical pumping case, not only the pump-induced population inversion gives rise to the optical gain, but the resonant Raman process in the quantum well also contributes to the gain.[10,11] This gain enhancement due to the Raman processes relaxes the requirement of population inversion, which is more difficult to achieve in the THz frequency range.

Previously, the optically pumped intersubband lasers were made of GaAs/AlGaAs quantum wells.[5,6] Since the conduction band offset of these quantum wells are usually small ($\sim$ 300 meV), $CO_2$ lasers were employed as pump sources.[5,6,8] Therefore, it is almost impossible to build a compact THz system based on $CO_2$ laser pumping. In this paper, we propose to use optically pumped InGaAs-AlAsSb-InP coupled quantum wells to generate THz radiation. The advantage of our quantum well design is that the large bandedge offset allows the conventional diode laser to be used as a pump source and that the pump laser and THz laser may be integrated eventually monolithically or by heterogeneous bonding. Owing to the large conduction band offset, the near-infrared intersubband transitions in InGaAs-AlAsSb double quantum wells have been recently demonstrated.[12]

We design a four-subband ($E_1$-$E_4$) THz laser consisting of a lattice-matched $In_{0.53}Ga_{0.47}As/AlAs_{0.56}Sb_{0.44}/InP/AlAs_{0.56}Sb_{0.44}/InP$ triple quantum well embedded in

$AlAs_{0.56}Sb_{0.44}$ barrier materials, as shown in Fig. 1. (The 4-level structures based on GaAs/AlGaAs triple[13] and step[14] quantum wells have been studied recently and shown to allow easier population inversion.) The quantum well structure is assumed to be modulation $n$-type doped. To obtain the eigenenergies and envelope wave functions of the QW, we solve the effective-mass Schrödinger equation coupled with Poisson equation. The exchange-correlation effect is included in the local-density approximation. The conduction band offsets between $AlAs_{0.56}Sb_{0.44}$ and $In_{0.53}Ga_{0.47}As$ and between $AlAs_{0.56}Sb_{0.44}$ and InP are 1.7 eV[12] and 1.376 eV, respectively. For a sheet concentration of n=$10^{11}$ $cm^{-2}$, the calculated self-consistent potential, the four energy levels, and the corresponding wave functions are shown in Fig. 1.

Let us now consider the situation where the quantum well is subjected to a pump field of angular frequency $\omega_p$ and a weak signal field of frequency $\omega$. The polarizations of both pump ($E_p$) and probe ($E_\omega$) fields are assumed to be along the well growth direction ($z$ axis). The pump photon energy is close to the energy spacing $E_{41}$ between the ground state and the highest lying subband, while the probe photon energy is in the vicinity of the subband separation $E_{43}$. In this case, both pump and probe fields do not resonantly couple subband $E_2$. Thus, we will not include polarizations involving this subband in the calculation of the pump-probe coherence for simplicity. However, we incorporate it into the calculation of the population distribution because its presence allows the electrons in subband $E_3$ to relax fast into subband $E_2$ through emission of LO phonons and these electrons finally jump to the ground state. To describe the probe field response of the quantum well system in the presence of a strong pump field, we start with the single-particle density-matrix formalism. Under the rotating-wave approximation (RWA), we obtain the following coupled equations for the steady-state electron distribution function ($f_i$) and the polarization ($\rho_{ij}$) between subbands $i$ and $j$ (for brevity, we drop the electron wave-vector index in our notation):[11,15]

$$2\mathrm{Im}[\Omega_{31}^*(\omega_p)\rho_{31}(\omega_p) + \Omega_{41}^*(\omega_p)\rho_{41}(\omega_p)] - \frac{f_1 - f_1^{\mathrm{F}}}{T_{cc}} + \frac{f_2}{\tau_{21}} + \frac{f_3}{\tau_{31}} + \frac{f_4}{\tau_{41}} = 0 \ , \qquad (1)$$

$$-\frac{f_2 - f_2^{\mathrm{F}}}{T_{cc}} + \frac{f_3}{\tau_{32}} + \frac{f_4}{\tau_{42}} - \frac{f_2}{\tau_{21}} = 0 \ , \tag{2}$$

$$-2\mathrm{Im}[\Omega_{31}^*(\omega_p)\rho_{31}(\omega_p)] - \frac{f_3 - f_3^{\mathrm{F}}}{T_{cc}} + \frac{f_4}{\tau_{43}} - \frac{f_3}{\tau_{32}} - \frac{f_3}{\tau_{31}} = 0 \ , \tag{3}$$

$$-2\mathrm{Im}[\Omega_{41}^*(\omega_p)\rho_{41}(\omega_p)] - \frac{f_4 - f_4^{\mathrm{F}}}{T_{cc}} - \frac{f_4}{\tau_{43}} - \frac{f_4}{\tau_{42}} - \frac{f_4}{\tau_{41}} = 0 \ , \tag{4}$$

$$D_{43}(\omega)\rho_{43}(\omega) = (f_3 - f_4)\Omega_{43}(\omega) + \rho_{13}(\omega - \omega_p)\Omega_{41}(\omega_p) - \rho_{41}(\omega + \omega_p)\Omega_{31}^*(\omega_p) \ , \tag{5}$$

$$D_{13}(\omega - \omega_p)\rho_{13}(\omega - \omega_p) = \rho_{43}(\omega)\Omega_{41}^*(\omega_p) - \rho_{41}^*(\omega_p)\Omega_{43}(\omega) \ , \tag{6}$$

$$D_{41}(\omega + \omega_p)\rho_{41}(\omega + \omega_p) = -\rho_{43}(\omega)\Omega_{31}(\omega_p) + \rho_{31}(\omega_p)\Omega_{43}(\omega) \ , \tag{7}$$

$$D_{31}(\omega_p)\rho_{31}(\omega_p) = (f_1 - f_3)\Omega_{31}(\omega_p) - \rho_{43}^*(0)\Omega_{41}(\omega_p) \ , \tag{8}$$

$$D_{41}(\omega_p)\rho_{41}(\omega_p) = (f_1 - f_4)\Omega_{41}(\omega_p) - \rho_{43}(0)\Omega_{31}(\omega_p) \ , \tag{9}$$

$$D_{43}(0)\rho_{43}(0) = \rho_{31}^*(\omega_p)\Omega_{41}(\omega_p) - \rho_{41}(\omega_p)\Omega_{31}^*(\omega_p) \ . \tag{10}$$

In Eqs. (5)-(10), only resonant terms are considered. Also, the optical nonlinearity for the pump field is included. That effect was neglected in our previous work.[11] $\Omega_{ij}(\omega, \omega_p) = (E_\omega, E_p)\mu_{ij}/\hbar$, $D_{ij}(\omega) = \omega + i\gamma_{ij} - E_{ij}/\hbar$; $\gamma_{ij}$ is the line broadening factor and $\mu_{ij}$ is the dipole moment. $T_{cc}$ and $\tau_{ij}$ are the intrasubband carrier-carrier scattering and intersubband relaxation times, respectively. The quantity $f_i^{\mathrm{F}}$ denotes the Fermi-Dirac distribution function of the QW without the pump light. It is easy to see from Eqs. (1)-(4) that the pump field induces an electron population redistribution that is coupled with the intersubband polarization. Thus, by solving Eqs. (1)-(10), we simutaneously obtain the electron distribution function as well as the off-diagonal element $\rho_{43}(\omega)$, which determines the optical gain of the THz probe field. Then we can calculate the THz gain following Ref. 11.

For the QW structure given in Fig. 1, we performed numerical studies of the THz gain spectra. In our calculations, the following parameters were used: $T_{cc}$=0.3 ps, $\tau_{21}$=1.5 ps, $\tau_{31}$=1.0 ps, $\tau_{41}$=1.2 ps, $\tau_{32}$=0.4 ps, $\tau_{42}$=1.3 ps, and $\tau_{43}$=1.5 ps.[5,14] Note that the ratio $\tau_{43}/\tau_{32}$ is about 4, which is consistent with the calculations.[16] The line broadening factors are $\hbar\gamma_{43}$=2.0 meV and $\hbar\gamma_{41} = \hbar\gamma_{31}$=3.0 meV.

To understand the role of the pump-probe coherence in the probe response of the QW, we show in Fig. 2 the THz gain spectra at different pump intensities obtained by neglecting pump-probe coherent interactions. Namely, the calculated optical gain in Fig. 2 results purely from the pump-induced population inversion. The pump photon energy used in Fig. 2 is $\hbar\omega_p = E_{41}$=0.7904 eV (1.57 $\mu$m) that is close to the wavelength of the conventional communication lasers. We see from Fig. 2 that the THz gain increases as the pump intensity is increased, and the peak gain appears at the probe photon energy equal to the transition energy $E_{43}$. It is also evident that the increase in the maximum gain becomes slower when the pump intensity becomes larger (see the inset of Fig. 2). This gain saturation behavior is a direct result of population inversion saturation at high pump intensities, as illustrated in Fig. 3. Note that there is a small difference in the pump intensity dependence of the population inversion for positive and negative pump detunings as shown in Fig. 3. This is due to the fact that slightly more electrons are pumped onto subband $E_3$ as the pump photon energy gets closer to $E_3$. The saturation behavior of the population inversion is pump frequency dependent.

In Fig. 4 we show the THz gain spectra for different pump intensities calculated with the pump-probe coherence included. As in Fig. 2, the pump photon energy is $\hbar\omega_p = E_{41}$. Comparing Figs. 2 and 4 we see that, for small pump intensities (say less than 0.2 MW/cm$^2$), the coherent pump-probe interaction enhances the THz gain. This is so because in the pump-probe scheme considered in this paper, the resonant Raman scattering in the QW gives rise to a Raman gain in addition to the gain due to the population inversion. Thus one would expect that the THz gain increases with an increase in the pump intensity because the Raman gain is increased as well. However, we see from Fig. 4 that the peak THz gain first

increases and then decreases when the pump intensity is increased. As the pump intensity is furtherly increased. the gain approaches to a constant value. We also see from Fig. 4 that the peak location in the gain spectra is blueshifted with increasing the pump intensity, which is not shown in Fig. 2. This is because of the pump-probe interaction induced shift effect that is neglected in Fig. 2.

In summary, we have proposed to use a near-infrared pumped InGaAs-AlAsSb-InP triple quantum well to obtain THz gain. Owing to the large conduction band offset of the QW structure, we show that the THz radiation can be generated with a near-infrared diode lasers around 1.55 $\mu$m. We optimized the QW design to enhance the pump-induced population inversion between the two lasing subbands by adding a subband with an energy separation to the lower lasing subband close to the LO phonon energy. The THz gain is calculated by including the pump-probe coherent interaction. We showed that resonant Raman scattering enhances the THz gain at low and moderate pump intensities. At the high pumping level, the THz gain becomes smaller because of pump-induced population redistribution and pump-probe coherent interactions. We finally stress that the THz devices proposed in this paper combine the following major advantages in a single design: optical coherent gain enhancement, maximized inversion due to the phonon resonant depopulation, and the near-infrared pumping. We hope this would lead us a step further in our efforts to realize a THz laser based on QW-intersubband transitions.

## ACKNOWLEDGMENTS

This work is partly supported by NASA Ames Research Center Director's Discretionary Fund. The authors thank professor S.-L. Chuang for useful discussions.

# REFERENCES


* Also at Arizona State University, Department of Electrical Engineering, Tempe, AZ 85287.

[1] R. F. Kazarinov and R. A. Suris, Sov. Phys. Semicond. **5**, 172 (1971).

[2] J. Faist, F. Capasso. D. Sivco, C. Sirtori, A. L. Hutchinson, S. N. G. Chu, and A. Y. Cho, Science **264**. 553 (1994).

[3] J. Faist, F. Capasso. D. Sivco, C. Sirtori, J. N. Baillargeon, A. L. Hutchinson, S. N. G. Chu, and A. Y. Cho. Appl. Phys. Lett. **68**, 3680 (1996).

[4] C. Sirtori, J. Faist. F. Capasso, D. Sivco, A. L. Hutchinson, and A. Y. Cho, Appl. Phys. Lett. **69**, 2810 (1996).

[5] O. Gauthier-Lafaye. P. Boucaud, F. H. Julien, S. Sauvage, S. Cabaret, J.-M. Lourtioz, V. Thierry-Mieg and R. Planel. Appl. Phys. Lett. **71**, 3619 (1997).

[6] O. Gauthier-Lafaye. F. H. Julien, S. Cabaret, J.-M. Lourtioz, G. Strasser, E. Gornik, M. Helm, and P. Bois, Appl. Phys. Lett. **74**, 1537 (1999).

[7] B. Xu, Q. Hu, and M. R. Melloch, Appl. Phys. Lett. **71**, 440 (1997).

[8] I. Lyubomirsky, Q. Hu, and M. R. Melloch, Appl. Phys. Lett. **73**, 3043 (1998).

[9] M. Rochat, J. Faist, M. Beck, U. Oesterle, and M. Illegems, Appl. Phys. Lett. **73**, 3724 (1998).

[10] J. B. Khurgin, G. Sun, L. R. Friedman, and R. A. Soref, J. Appl. Phys. **78**, 7398 (1995).

[11] A. Liu and C. Z. Ning, Appl. Phys. Lett. **75**, 1207 (1999).

[12] A. Neogi, T. Mozume, H. Yoshida, and O. Wada, IEEE Photonics Technol. Lett.**11**, 633 (1999).

[13] I. Lyubomirsky and Q. Hu, Appl. Phys. Lett. **73**, 300 (1998).

[14] P. Kinsler, P. Harrison, and R. W. Kelsall, J. Appl. Phys. **85**, 23 (1999).

[15] A. Liu, J. Opt. Soc. Am. B **15**, 1741 (1998).

[16] P. Harrison, R. W. Kelsall, P. Kinsler, and K. Donovan, in: *1998 IEEE Sixth International Conference on Terahertz Electronics Proceedings*, ed. by P. Harrison (1998), pp. 74-78.

## FIGURES

FIG. 1. Self-consistent potential and the four lowest energy levels with corresponding wave functions of an $In_{0.53}Ga_{0.47}As/AlAs_{0.56}Sb_{0.44}/InP/AlAs_{0.56}Sb_{0.44}/InP$ triple quantum well structure. $In_{0.53}Ga_{0.47}As$ well width is 3.9 nm and InP well width is 2.0 nm. The thicknesses of the wider and narrower barrier layers are 4.0 and 3.0 nm, respectively. The calculated transition energies ($E_{ij}$) and dipole matrix elements ($Z_{ij}$) are $E_{43}$=20.7 meV, $E_{32}$=40.4 meV, $E_{41}$=790.4 meV, $Z_{21}$=0.98 Å, $Z_{31}$=3.2 Å. $Z_{41}$=9.6 Å, $Z_{32}$=26.2 Å, $Z_{42}$=0.17 Å, and $Z_{43}$=25.3 Å.

FIG. 2. THz gain spectra without pump-probe coherence for different pump intensities. The maximum gain as a function of the pump intensity is shown in the inset.

FIG. 3. Population difference versus the pump intensity at different pump detunings, i.e., $\hbar\omega_p - E_{41}$=-6, -3, 0, 3. and 6 meV.

FIG. 4. THz gain spectra with pump-probe coherence for different pump intensities.

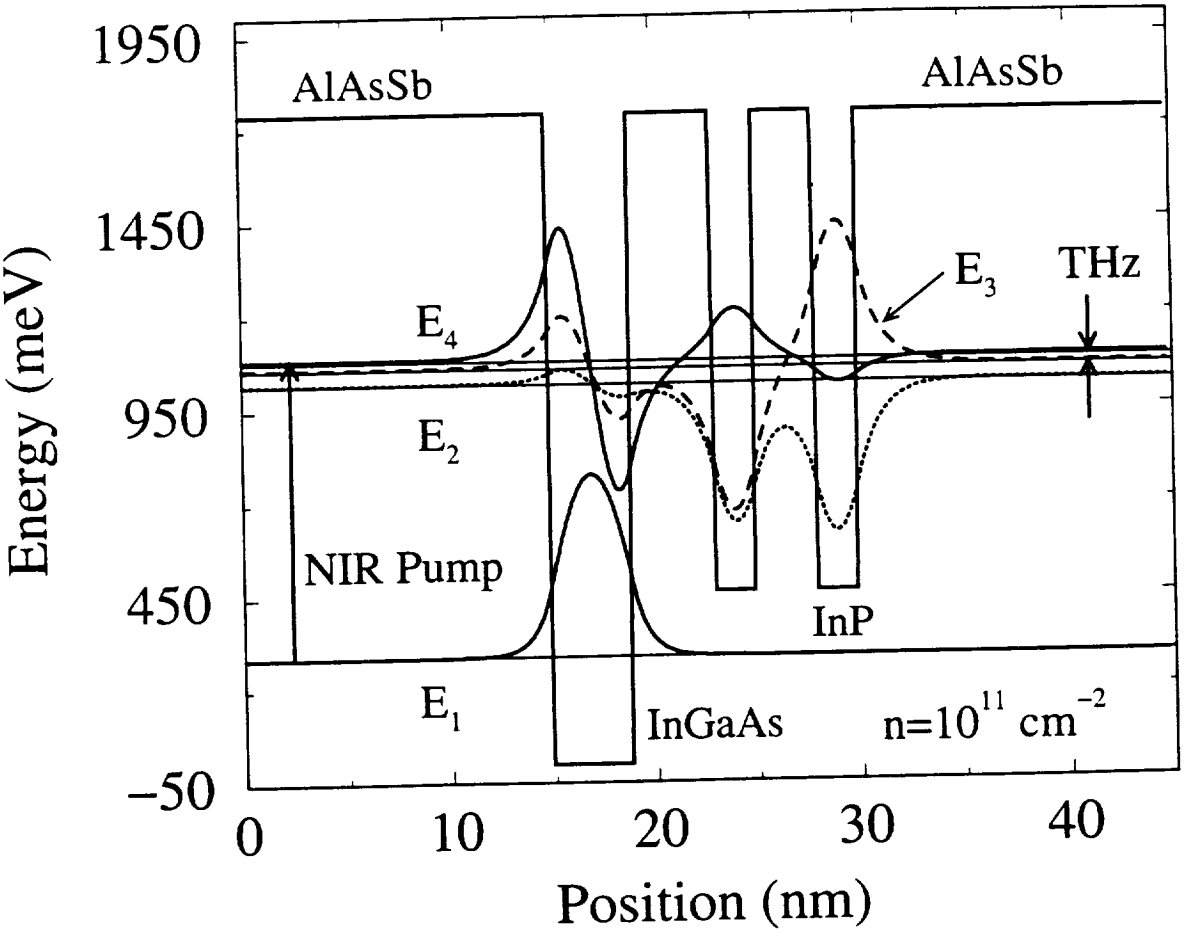
1950
1450
950
450
−50
Energy (meV)
AlAsSb
AlAsSb
E4
E3
THz
E2
NIR Pump
InP
E1
InGaAs
n=10^11 cm^-2
0
10
20
30
40
Position (nm)

FIG. 1.

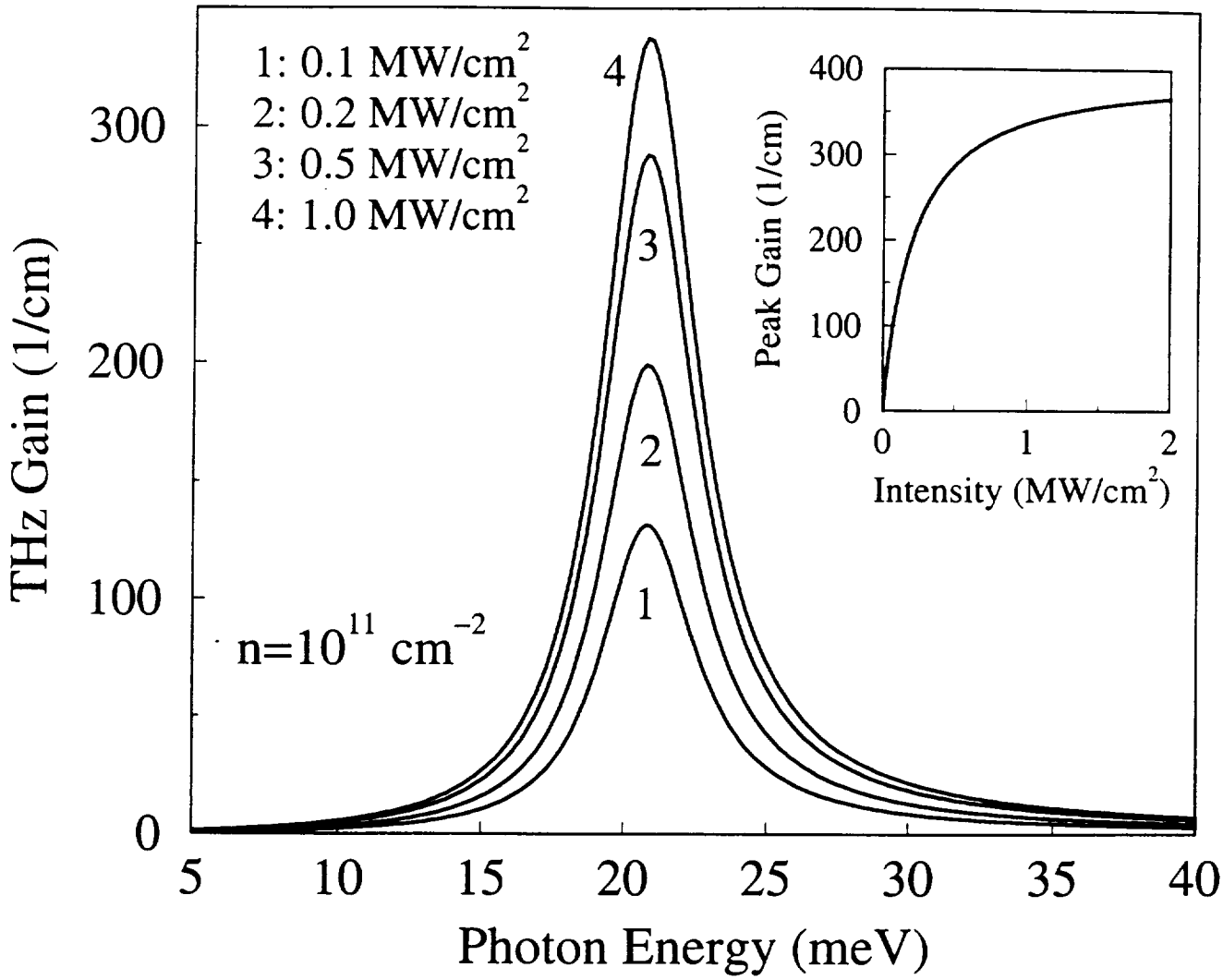
1: 0.1 MW/cm$^2$
2: 0.2 MW/cm$^2$
3: 0.5 MW/cm$^2$
4: 1.0 MW/cm$^2$
n=10$^{11}$ cm$^{-2}$
THz Gain (1/cm)
Photon Energy (meV)
Peak Gain (1/cm)
Intensity (MW/cm$^2$)

FIG. 2.

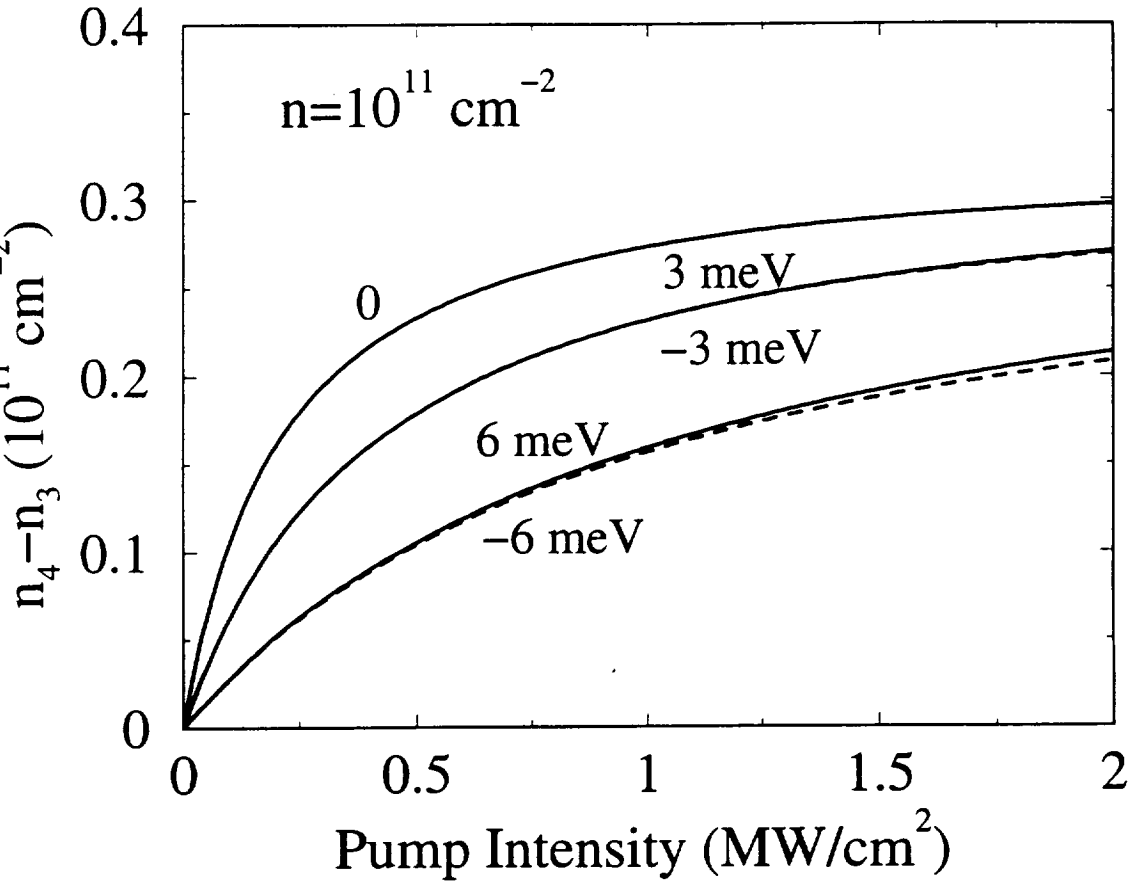
0.4
0.3
0.2
0.1
0
n=10^11 cm^-2
0
3 meV
−3 meV
6 meV
−6 meV
n4−n3 (10^11 cm^-2)
0
0.5
1
1.5
2
Pump Intensity (MW/cm^2)

FIG. 3.

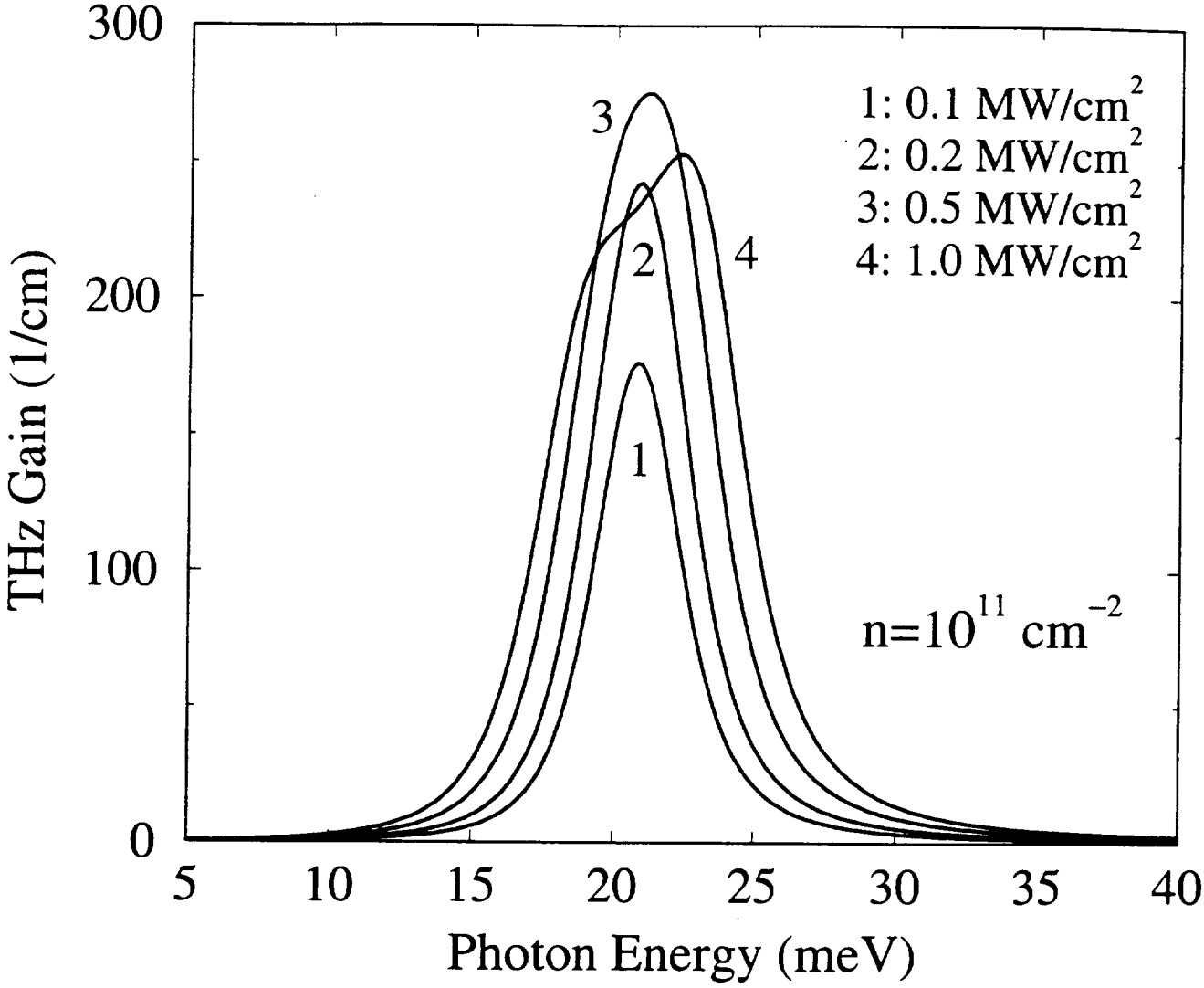
300
200
100
0
THz Gain (1/cm)
5
10
15
20
25
30
35
40
Photon Energy (meV)
1: 0.1 MW/cm2
2: 0.2 MW/cm2
3: 0.5 MW/cm2
4: 1.0 MW/cm2
n=10^11 cm^-2
1
2
3
4

FIG. 4.